Desalination and Water Treatment
www.deswater.com

doi: 10.1080/19443994.2014.985730

57 (2016) 3720–3731
February

Taylor & Francis
Taylor & Francis Group

Synthesis of mesoporous material SBA-3 for adsorption of dye congo red

Seema Rani, Kaur Sumanjit*, R.K. Mahajan

Department of Chemistry, Guru Nanak Dev University, Amritsar 143005, India, Tel. +91 183 2256818; Fax: +91 183 2258820; emails: knathiyaseema@yahoo.com (S. Rani), sumangndu@yahoo.co.in (K. Sumanjit), rakesh_chem@yahoo.com (R.K. Mahajan)

Received 20 August 2014; Accepted 2 November 2014

ABSTRACT

Mesoporous material SBA-3 was synthesized and used as an adsorbent for the removal of dye congo red from aqueous solutions. Adsorbent was characterized by Fourier transform infrared spectroscopy, X-ray diffraction, scanning electron microscopy, and N_2 adsorption–desorption and depicted the surface area of 690 $m^2 g^{-1}$. Adsorptions conditions were optimized by analyzing the effect of contact time, initial dye concentration, adsorbent dose, pH, and temperature. Experimental data were contemplated for various kinetics and thermodynamics models at different concentrations and corroborated that adsorption process is second order at all studied concentrations. Langmuir model imparted high value of monolayer capacity of 344.8 mg g^{-1} for SBA-3. Thermodynamic parameters insinuated that present adsorption process is feasible, spontaneous, and exothermic in nature.

Keywords: Adsorption; Congo red; SBA-3; Kinetics; Isotherm

1. Introduction

The dye pollution originating from the textile, paper, printing, leather, and other industries is considered as a significant source of aquatic ecosystem disequilibria [1]. Increasing environmental pollution caused by toxic dyes due to their hazardous nature is a matter of great concern. Even small traces of the non-biodegradable and highly toxic dyes can prove harmful to the mankind [2]. Color effluents discharged from dye production industries not only degrade the esthetic value of the water bodies but also interfere with the penetration of light into the water, thereby leading to disturbances in the aquatic ecosystem [3]. Unfortunately, the toxic dyes once pass into the wastewater cause detrimental effects on the human/animal health, which are not only limited to themselves but may be passed on to further generation by the way of genetic mutations, birth defects, inherited diseases, and so on [4]. Approximately 70% of the synthetic dyes belong to the azo group which contains N=N bond in there molecular structure. These dyes may undergo oxidation, hydrolysis, and many other chemical reactions which may result in the production of toxic by-products which are harmful to the environment [5–7]. Dye congo red (CR) is a derivative of benzidine and napthoic acid and metabolizes to carcinogenic products. It is investigated as a mutagen and reproductive effector. It is a skin, eye, and gastrointestinal irritant. It may affect blood factors such as clotting, and induce somnolence and respiratory problems [8]. Although CR, a human carcinogen, has been banned in many countries due to health hazards, but it is still consumed in several countries [8,9]. Removal of these dyes from aquatic environment is strongly

*Corresponding author.

recommended and still a challenging issue for the researcher.

Several methods such as physical, chemical, and biological approaches have been reported for the removal of dye materials from wastewater to reduce their adverse effects on environment. Among these methods, adsorption has been found to be an efficient, effective, simple and economic process to remove dyes from wastewater without leaving behind any toxic by-product [10–12]. Activated carbon is used as an adsorbent because of its high adsorption capacity but its use is limited due to its high cost. Various researchers have studied the application of industrial waste, natural material, or agricultural byproducts as adsorbents for dye removal because these materials are inexpensive, simple, and abundantly available [13–18]. Recently, new mesoporous materials are synthesized to improve their adsorption performance. Highly porous materials offer a number of potential advantages as adsorbents including larger pore volume and diameter, high surface area and regular channel type structures.

Zhao et al. [19] reported a mesoporous material named SBA, with uniform hexagonal structure. It was synthesized using a low molecular weight alkyl quaternary ammonium template at room temperature and under acidic condition. Mesoporous silica SBA-3 has a negative charge density due to the presence of Si–O and Si–OH groups, which adsorb positively charged dyes and prevent the adsorption of negative ones [20]. Without removal of surfactant template showed good adsorption capacity for azo dye CR from their aqueous solutions. This study reports the adsorption of CR from aqueous solutions on mesoporous material SBA-3. The adsorption behavior of the dye as a function of temperature, pH, and shaking time were studied. The kinetic parameters were calculated to determine the adsorption mechanism. Nature of the adsorption process was studied using various thermodynamics parameters related to the adsorption of dye such as free energy change (ΔG), enthalpy change (ΔH), and entropy change (ΔS).

2. Materials and methods

Tetraethylorthosilicate (TEOS) was purchased from Sigma (Aldrich). Ethanol, sodium hydroxide, and hydrochloric acid were procured from Merck, India. *n*-Cetyl trimethylammonium bromide (CTAB, chemical formula = $C_{19}H_{42}BrN$, Mol. wt. = 364.45) was purchased from SD Fine chemical, India, and dye CR [chemical formula = $C_{32}H_{22}N_6Na_2O_6S_2$, FW = 696.68, λ_{max} = 497 nm] is a benzidine-based anionic disazo dye, i.e. a dye with two azo groups was supplied by Thomas Baker, Mumbai, India.

2.1. Adsorbate

An accurate weighed quantity of the dye CR was dissolved in double-distilled water to prepare a stock solution (1,000 mg L^{-1}). Desired concentrations were obtained by successive dilutions with double-distilled water.

2.2. Synthesis of SBA-3

The mesoporous material SBA-3 was synthesized using the method reported in the literature [21]. During the synthesis of SBA-3, TEOS was used as silica source and CTAB as a template. The aqueous solution of HCl (37%) was used to maintain the acidic conditions. One gram of CTAB was dissolved in 50 mL deionized water and 15 mL of HCl with stirring for 30 min. Five milliliters of TEOS was added drop wise to the acidic CTAB solution with stirring at room temperature. Solution was stirred for further 2 h and left to aging for 12 h in Teflon container. The resulting solution was heated at 150°C for two days. White material obtained was filtered and washed with distilled water and ethanol and dried at 100°C overnight.

2.3. Characterization

FTIR spectra of the samples were recorded in a Perkin Elmer FTIR spectrophotometer in the range of 400–4,000 cm^{-1} taking KBr as the reference. Surface morphology was studied by scanning electron microscope (Carl Zeiss Supra 55), equipped with energy dispersive X-ray analysis (EDX) using gold sputtering process. The material is further characterized using the X-ray diffraction in the scanning mode on XRD 7000 (Shimadzu, Japan) analytical instrument operated at 40 kV and a current of 30 mA with Cu-Kα radiation (λ = 1.5406 Å). The N_2 adsorption–desorption isotherms of the adsorbent was measured using an automatic adsorption instrument (Micromeritics Chemisorb ASAP 2020) at liquid nitrogen temperature (77 K). Prior to measurements, sample was degassed at 300°C for 12 h under vacuum. The specific surface area (SBET) of the adsorbent was calculated using the Brunauer–Emmett–Teller (BET) equation by assuming the area of the nitrogen molecule to be 0.162 nm^2. The total pore volumes were estimated from the liquid volume of adsorbate adsorbed (N_2) at a relative pressure of 0.99. In addition, the pore size distribution was determined using the Barrett–Joyner–Halenda (BJH) method applied on the adsorption/desorption hysteresis loop assuming a model of cylindrical open-ended pores.

2.4. Adsorption studies

CR removal capacity of the SBA-3 was investigated in a batch system. Ten milligrams of the adsorbent was added to 25 mL CR solution of known concentration and agitated at 150 rpm in a shaker (metrex orbital shaker) at different temperatures. Experiments were carried out for equilibrium time to ensure that equilibrated adsorption was obtained, except for kinetic study where the samples were withdrawn from the experimental flask at predetermined time intervals. After the equilibration period, the mixture was centrifuged using Eltek centrifuge (TC 450 D) for 5 min at 4,000 rpm. Concentration of dye in the supernatant solution before and after the adsorption was determined with a UV–visible spectrophotometer (1800, Shimadzu, Japan) at a wavelength of maximum absorption (λ_{max}).

Adsorption capacity, q_t (mg g^{-1}), of the adsorbent was calculated by a mass balance relationship, which represents the amount of dye adsorbed per amount of adsorbent: $q_t = V\,(C_o - C_t)/m$, where C_o is the initial dye concentration (mg L^{-1}), C_t is the dye concentration in solution (mg L^{-1}) at time t, V is the volume of the solution (L), and m is the mass of the mesoporous SBA-3 (g). The percent removal (%) of dye was calculated using the equation: % removal $= [(C_o - C_t)/C_o] \times 100$.

3. Results and discussion

3.1. Characterization of SBA-3

The XRD spectrum was used to investigate the mesoporous structure of SBA-3. The well resolved peaks at $2\theta = 2.2$ (figure not shown) in XRD patterns of SBA-3 demonstrate the hexagonally ordered structure, which is indicative of well ordered mesoporous structure and crystalline nature of mesoporous material. Average crystallite size calculated using the Scherrer's equation was found to be 14.3 nm. Morphology of SBA-3 is given by SEM images and depicted the formation of spherical nanoparticles (Fig. 1). However the EDX scanning imparted the presence of carbon,

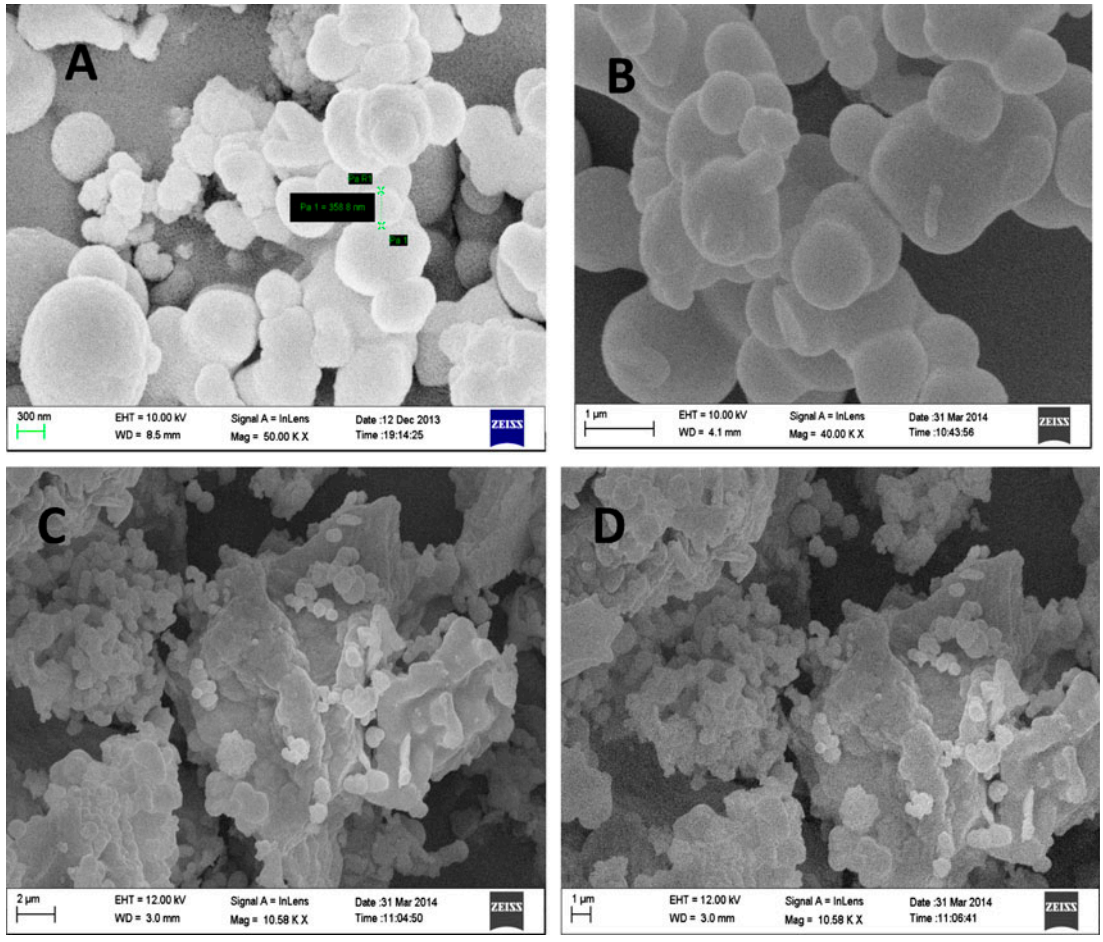

Fig. 1. SEM images of SBA-3 before dye loading (A, B) and after loading of dye CR (C, D) at different scales.

oxygen, and silicon contents. The FTIR spectrum of mesoporous material SBA-3 was recorded over the range of 4,000–400 cm^{-1} (figure not shown). A broad band in the range of 3,700–3,010 cm^{-1} is seen which can be attributed to the framework of Si–OH group interaction with adsorbed water molecules. The Si–OH peak appears at about 3,459 cm^{-1}. The asymmetric stretching vibrations of Si–O–Si and Si–OH are observed by the absorption bands at 1,084 cm^{-1}, and the band at 797 cm^{-1} is assigned to free silica. Similar peaks are also observed by other workers [20].

Nitrogen adsorption studies carried out where the isotherms can be classified as type IV isotherms according to the IUPAC nomenclature (Fig. 2). A linear increase of absorbed volume at low pressures is followed by a steep increase in nitrogen uptake at a relative pressure of $0.34 < p/p_0 < 0.45$, which is due to capillary condensation inside the mesopores. The long plateau at higher relative pressures indicates that pore filling is restricted to the inflection point at $p/p_0 = 0.34$ for SBA-3. A steep increase occurs in nitrogen uptake and an adsorbed hysteresis loop appears at a relative pressure $0.9 < p/p_0 < 1.0$. According to BET method, the SBET and pore volume are estimated to be 690 $m^2 g^{-1}$ and 0.17–0.23 $cm^3 g^{-1}$, respectively. BJH method was applied to calculate the pore size distribution. The average diameter of pores in SBA-3 calculated with BJH method is about 3.5–4.4 nm.

3.2. Adsorption experiments

3.2.1. Effect of contact time

The contact time between adsorbate and adsorbent is one of the most important parameters that affect the performance of adsorption processes. Adsorption process followed two phases first initially the rapid phase where adsorption capacity increases sharply due to external surface adsorption, second the slower phase where adsorption capacity increases slowly due to internal surface adsorption [22]. Fig. 3 shows removal efficiencies for the dye CR as a function of time. Results described that the curves are single, continuous, and smooth and leading to saturation during the sorption process, suggesting the possible monolayer coverage of CR onto SBA-3 at all studied concentrations.

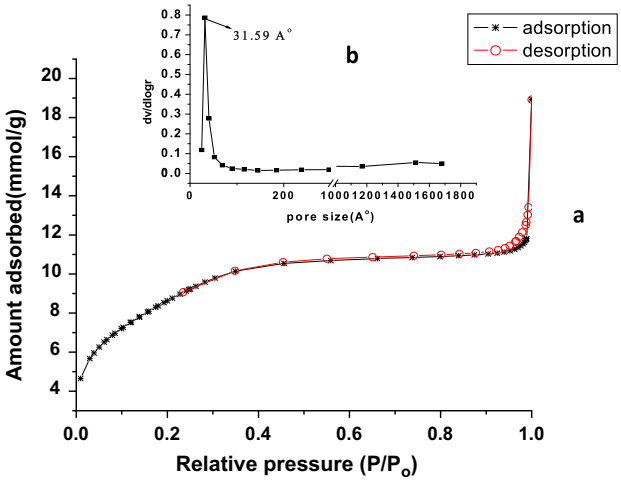

Fig. 2. (a) Nitrogen adsorption–desorption isotherm and (b) pore size distribution of SBA-3.

3.2.2. Effect of initial concentration

Fig. 4 illustrates the effect of initial concentration of dye for adsorption of CR onto SBA-3. It is clear from the figure that the percentage CR removal decreased with the increase in initial concentration of CR. At higher initial concentration the percentage removal decreases because the availability of adsorption sites is less. However, the adsorption capacity increases with increase in initial dye concentration. It may be due to the increase in the number of dye molecules competing for the available binding sites on the surface of the adsorbent. The initial dye concentration provides the necessary driving force to overcome the resistance to the mass transfer of CR between aqueous phase and the solid phase [23]. The mass transfer driving force becomes larger with increase in initial dye concentration which results the higher sorption for CR. Consequently, a higher initial concentration of dye solution can promote the sorption process. In addition, increase of initial acid dye concentration increases the number of collisions between acid dye anions and adsorbent, which enhances the sorption process.

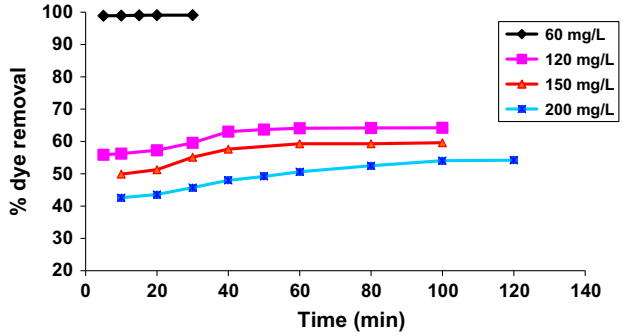

Fig. 3. Effect of contact time on the adsorption of CR onto SBA-3 at 303 K at various initial concentration of dye (adsorbent dose = 0.4 g L^{-1}, pH 7).

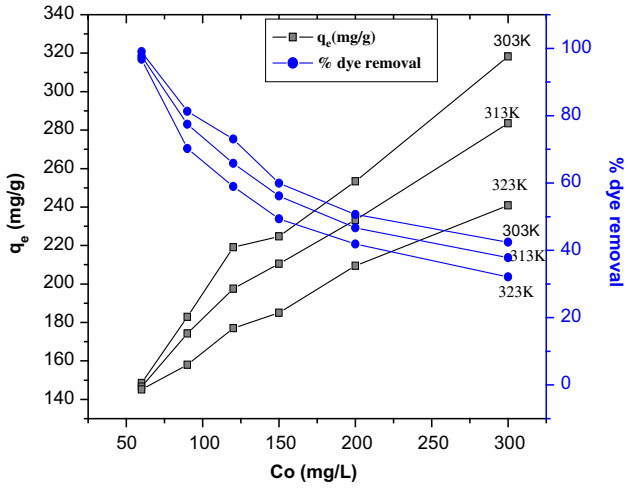

Fig. 4. Effect of initial dye concentration on the adsorption of dye CR onto SBA-3 (adsorbent dose = 0.4 g L^{-1}, pH 7.0).

3.2.3. Effect of adsorbent dose

Study of the effect of adsorbent dosage gives an idea of the effectiveness of an adsorbent and the ability of a dye to be adsorbed with a minimum dosage. The effect of SBA-3 dosage on CR adsorption was studied at 30°C at initial dye concentration of 200 mg L^{-1}. With increase of adsorbent dosage from 0.4 to 1.2 g L^{-1}, the removal of CR increased from 54.4 to 99.7% (Fig. 5). The increase in percentage of dye removal with increasing adsorbent dosages is due to increase of sorption active sites at the adsorbent surface. The decrease in adsorption capacity, q_e (mg g^{-1}), with increasing adsorbent mass is due to the split in the flux or the concentration gradient between solute concentration in the solution and the solute concentration on the surface of the adsorbent [24,25].

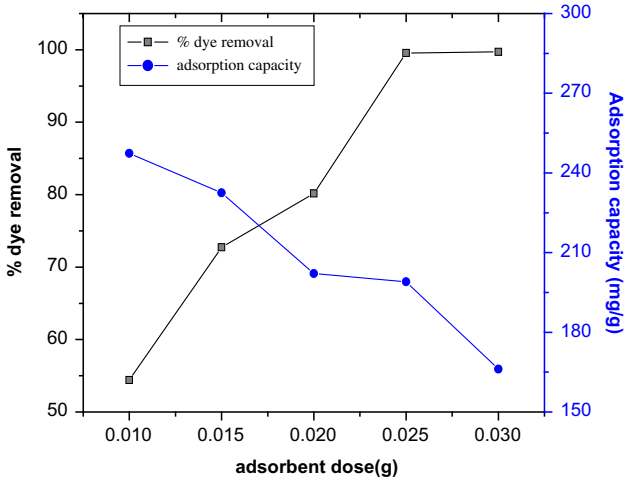

Fig. 5. Effect of adsorbent dose on the adsorption removal of CR onto SBA-3 (pH 7.0, C_o = 200 mg L^{-1}).

3.2.4. Effect of pH

The initial pH of the dye solution is recognized as an important operational parameter which can significantly affect the adsorption mechanisms between the dye molecules and the adsorbent. The dye CR is an indicator dye, changes its color from red to blue in the presence of acids and from red to dark red that is different from original red in the presence of base. The effect of pH on the present adsorption system was studied. The adsorption increased gradually from 46.8 to 99.1% with decrease in pH from 12 to 2.0. It is evident that the maximum removal of dye absorbed is at pH 2 (Fig. 6). Low pH leads to an increase in H^+ ion concentration in the system, and the surface of the SBA-3 acquires positive charge by adsorbing H^+ ions. As the SBA-3 surface is positively charged at low pH, a significantly strong electrostatic attraction appears between the positively charged sites and dye anion. Lower adsorption of the CR in alkaline medium is also due to the competition between excess OH^- ions and the anionic CR dye molecule for the adsorption sites.

3.2.5. Effect of temperature

Fig. 4 illustrates the equilibrium removal of dye CR as a function of temperature, for experiments conducted at different concentrations. The temperature is an important parameter in the context of adsorption on solid phase and has two major effects on the adsorption process. Increasing the temperature is known to increase the rate of diffusion of the adsorbate molecules across the external boundary layer and

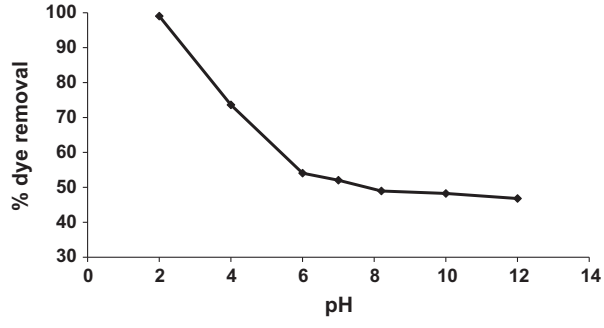

Fig. 6. Effect of pH on the adsorption removal of CR onto SBA-3 (adsorbent dose = 0.4 g L^{-1}, C_o = 200 mg L^{-1}).

in the internal pores of the adsorbent particle, owing to decrease in the viscosity of the solution. In addition, changing temperature will change the equilibrium capacity of the adsorbent for a particular adsorbate [26]. For this study, it was found that percentage removal as well as adsorption capacity decreases with increase in temperature. Reduction of adsorption capacity of dye at higher temperatures may be attributed to the deactivation of the adsorbent surface. This fact demonstrated an exothermic adsorption process [27]. This may be due to the physical bonding between dye molecules and the active sites of the adsorbent. It is weakened as temperature increased, whereas, the solubility of dyes increased thus interaction forces between the solute and the solvent become stronger than those between solute and adsorbent, making the solute more difficult to adsorb. The adsorption is favored by a decrease in temperature, a phenomenon which is also characteristic of physical adsorption.

3.2.6. Adsorption kinetics

Adsorption behavior of CR is analyzed using the Lagergren first-order kinetic model, pseudo-second-order kinetic model, intraparticle diffusion, and Elovich and Bangham model as most applicable kinetic models.

3.2.6.1. Lagergren first-order model. The linear form of this equation is given as:

$$\log(q_e - q_t) = \log q_e - \frac{k_f}{2.303}t \quad (1)$$

where q_e and q_t (mg g^{-1}) are the amount of dye adsorbed at equilibrium and at time t (min), respectively, k_f (min^{-1}) is the rate constant of Langergren first-order adsorption. The respective value of kinetic model parameters is calculated for slope and intercept of obtained straight line, and their values are presented in Table 1. The q_e values calculated from the model does not agree well with q_e (experimental) values. It implies that adsorption does not follow first-order kinetic model.

3.2.6.2. Pseudo-second-order model. The kinetic data are further analyzed using the pseudo-second-order kinetic model expressed as:

$$\frac{t}{q_t} = \frac{1}{k_s q_e^2} + \frac{1}{q_e}t \quad (2)$$

where k_s (g mg^{-1} min^{-1}) is the rate constant of pseudo-second-order adsorption. The liner plots of t/q_t vs. t with high correlation coefficient show the applicability of this model for interpretation of experimental data. The second-order kinetic model parameters were evaluated from plot, and their values are included in Table 1. It is seen that the experimental values of $q_{e,\exp}$ are in good agreement with theoretical values

Table 1
Kinetic parameters for the removal of CR onto SBA-3 at different initial concentrations

Equations	Parameters	Concentration of dye (mg L^{-1})			
		60	120	150	200
Pseudo first order	q_e exp (mg g^{-1})	148.57	196.06	221.08	245.64
	q_e cal (mg g^{-1})	0.73	82.87	159.96	109.90
	k_f (min^{-1})	0.14	0.09	0.08	0.04
	R^2	0.89	0.89	0.95	0.95
Pseudo-second-order	q_e exp (mg g^{-1})	148.57	196.06	221.08	245.64
	q_e cal (mg g^{-1})	149.25	200	227.27	263.15
	k_s (g mg^{-1} min^{-1})	0.45	0.0027	0.0014	0.0005
	R^2	0.99	0.99	0.99	0.99
Intra-particle diffusion	k_{id} (mg g^{-1} min$^{-1/2}$)	0.15	6.12	8.79	9.40
	C (mg g^{-1})	147.9	150.69	151.45	155.35
	R^2	0.97	0.98	0.99	0.98
Elovich	a	1.17×10^{275}	1.67×10^{5}	6.8×10^{3}	1.7×10^{3}
	b	4.29	0.069	0.045	0.036
	R^2	0.93	0.96	0.95	0.96
Bangham	k_o (g)	263.1	488.6	743.7	1,087.9
	α	0.03	0.10	0.16	0.17
	R^2	0.92	0.94	0.97	0.97

calculated ($q_{e,\mathrm{cal}}$) from the pseudo-second-order equation. Therefore, it is concluded that the pseudo-second-order kinetic model provides a better correlation for the adsorption of CR on SBA-3.

3.2.6.3. Weber–Morris intraparticle diffusion equation. External diffusion and internal diffusion (or intraparticle diffusion) are the two stages for the adsorption process on a porous adsorbent [28]. An empirically found functional relationship common to most adsorption process is that the uptake varies almost proportionally with $t^{½}$, the Weber–Morris plot (q_t vs. $t^{1/2}$), rather than with the contact time, t [29].

$$q_t = k_{\mathrm{id}} t^{1/2} + C \tag{3}$$

k_{id}, the internal diffusion intraparticle transport parameter constant (mg g^{-1} min$^{-0.5}$) can be obtained from the slope of the q_t vs. $t^{1/2}$ plot and is listed in Table 1. If the Weber–Morris plot of q_t vs. $t^{1/2}$ satisfies the linear relationship with the experimental data, then the sorption process is found to be controlled by intra-particle diffusion only. Generally, it has been proposed that adsorption consists of three steps. The first, sharper portion is attributed to the diffusion of adsorbate through the solution to the external surface of adsorbent or boundary layer diffusion of solute molecules. The second describes the gradual equilibrium stage with intra-particle diffusion dominating. The third portion is attributed to the final equilibrium stage for which the intra-particle diffusion starts to slow down due to the extremely low adsorbate concentration left in the solution [30,31].

To exactly deduce the experimental findings, sorption data were given a quantitative treatment based on the model proposed by Boyd et al. and Richenberg [32,33] and various parameters were calculated using the following equations:

$$F = 1 - \frac{6}{\Pi^2}\exp(-\mathrm{Bt}) \tag{4}$$

where F is the fractional attainment of equilibrium at time "t," and Bt is a mathematical function of F. The F (fractional attainment) is acquired by applying following equation:

$$F = \frac{q_t}{q_e} \tag{5}$$

where q_t (mg g^{-1}) and q_e (mg g^{-1}) are amounts adsorbed after time t and at equilibrium time, respectively. Substituting Eq. (5) into Eq. (4), the kinetic expression becomes as follows:

$$\mathrm{Bt} = -0.4977 - \ln\left(1 - \frac{q_t}{q_e}\right) \tag{6}$$

Eq. (6) is used to calculate Bt values. The calculated Bt values were then plotted against time as shown in Fig. 7. From this plot, it is possible to identify whether external transport or intraparticle diffusion controls the rate of adsorption. If a plot of Bt vs. t is a straight line passing through the origin, then adsorption will be governed by a particle-diffusion mechanism (transport of the adsorbate within the pores of the adsorbent), otherwise governed by film diffusion (transport of adsorbate to the surface of the adsorbent) [34]. From Fig. 7, it is observed that the plot has desirable linear form at higher concentration, and almost passing through origin which indicates the ongoing adsorption processes to be governed by particle-diffusion mechanism, whereas at lower dye concentration 60 mg L^{-1}, process is controlled by film diffusion.

3.2.6.4. Elovich model. A kinetic equation of chemisorptions was used to describe the rate of adsorption that decreases exponentially with an increase in the amount of adsorbate named Elovich equation and it is generally expressed as [35]:

$$q_t = \frac{1}{b}\ln(ab) + \frac{1}{b}\ln t \tag{7}$$

where a and b are constants. The constant a, is considered as the initial sorption rate (mg g^{-1} min^{-1}), and b is related to the extent of surface coverage and activation energy for chemisorptions (g mg^{-1}), and q_t (mg g^{-1}) is the amount of dye adsorbed at time t (min).

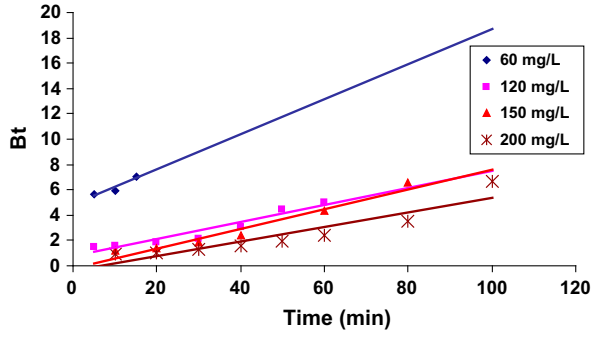

Fig. 7. Correlationship of Bt vs. time (min) on the adsorption of CR onto SBA-3 at various initial concentration of dye (adsorbent dose = 0.4 g L^{-1}, pH 7.0).

The values of a and b obtained from the linear plots of q_t vs. ln t are comprised in Table 1.

3.2.6.5. Bangham's equation. Kinetic data were further used to know about the slow step occurring in the present adsorption system using Bangham's equation [36].

$$\text{Log } \log(C_o/C_o - q_t m) = \log(k_o m/2.303V) + \alpha \log t \quad (8)$$

where C_o is the initial concentration of dye in solution (mg L^{-1}). V is the volume of the solution (ml), m is the weight of adsorbent per liter of solution (g L^{-1}). q_t (mg g^{-1}) is amount of dye adsorbed at time t, and α (<1) and k_o are constants and are accommodated in Table 1. Linear plot (Log log ($C_o/C_o - q_t m$) vs. log t) demonstrated that the diffusion of adsorbate into pores of adsorbents is not the only rate controlling step [37].

3.2.7. Adsorption equilibrium isotherms

Five isotherm equations have been tested in this study.

3.2.7.1. Langmuir model. The Langmuir isotherm is based on the assumption of a structurally homogeneous adsorbent and the monolayer coverage. That is, once a dye molecule occupies a site, no further adsorption can take place at that site

$$C_e/q_e = C_e/C_m + 1/K_L\, C_m \quad (9)$$

where C_e (mg L^{-1}) is the equilibrium concentration of the adsorbate, q_e (mg g^{-1}) is the amount adsorbed at equilibrium, and C_m (mg g^{-1}) and K_L (L mg^{-1}) are constants related to the adsorption capacity and energy of adsorption, respectively. The Langmuir constants K_L and C_m can be determined from the linear plot of C_e/q_e vs. C_e, Table 2. Maximum adsorption capacity was found to be 344.8, 312.5, and 263.2 mg g^{-1} at 303, 313, and 323 K, respectively. Values of C_m decreases with increase in temperature suggesting the exothermic nature of adsorption process. According to Hall et al., the favorable adsorption of the Langmuir isotherm can be expressed in terms of a dimensionless constant separation factor or equilibrium parameter R_L. $R_L = 1/(1 + K_L C_o)$, where C_o (mg L^{-1}) is the initial dye concentration of dye. The value of parameter R_L indicates the nature of the adsorption process. (i) $R_L > 1$ for unfavorable adsorption, (ii) $R_L = 1$ for linear adsorption, (iii) $0 < R_L < 1$ for favorable adsorption, and (iv) $R_L = 0$ for irreversible adsorption. The value of R_L (Table 3) for the present system comes out to be less than one at all studied temperature communicating the favorable adsorption of dye CR onto SBA-3.

3.2.7.2. Freundlich isotherm. The Freundlich isotherm describes the non-ideal adsorption of a heterogeneous system and reversible adsorption. The linear form of Freundlich equation can be expressed as.

$$\log q_e = \log K_F + 1/n \log C_e \quad (10)$$

Table 2
Isotherm parameters for the removal of CR onto SBA-3 at different temperatures

Equations	Parameters	Temperature (K)		
		303	313	323
Langmuir	K_L (L mg^{-1})	0.043	0.040	0.039
	C_m (mg g^{-1})	344.8	312.5	263.15
	R^2	0.97	0.98	0.99
Freundlich	K_F (mg g^{-1}) (L $mg^{-1})^{1/n}$	98.78	90.19	79.10
	n	4.63	4.74	4.86
	R^2	0.93	0.96	0.98
Tempkin	K_T (L mg^{-1})	1.74	1.69	1.64
	B_1	52.32	46.88	40.20
	b_T (kJ mol^{-1})	0.048	0.055	0.067
	R^2	0.94	0.98	0.96
Dubinin Radushkevich	q_s (mg g^{-1})	263.0	239.2	211.8
	E (kJ mol^{-1})	0.26	0.23	0.21
	R^2	0.89	0.84	0.80
NICA	N	0.46	0.49	0.61
	K_G (mg L^{-1})	3.17	3.62	5.20
	R^2	0.98	0.93	0.94

Table 3
Thermodynamic parameters for the adsorption of CR onto SBA-3 at different temperatures

Temperature (K)	R_L values	$-\Delta G$ (kJ mol^{-1})	ΔH (kJ mol^{-1})	ΔS (J mol^{-1} K^{-1})
303	0.279	25.96	–3.9	72.46
313	0.294	26.64		
323	0.299	27.42		

where q_e is the amount adsorbed (mg g^{-1}), and C_e is the equilibrium concentration of the adsorbate (mg L^{-1}). K_F (mg g^{-1}) (L g^{-1})$^{1/n}$ and n, the Freundlich constants, are related to adsorption capacity and adsorption intensity, respectively. Freundlich constant n is a measure of the deviation from linearity of the adsorption. If a value for n is equal to unity, the adsorption is linear. Value of n below unity implies that adsorption process is chemical, but if a value for n is above unity, adsorption is favorable, a physical process [38]. Values of Freundlich constants (K_F and n) are presented in Table 2. Value of n is greater than unity at all temperatures, thereby indicating physical adsorption process of the dye CR for SBA-3. K_F values decreased with increasing temperature, thereby indicating that dye–adsorbent interaction weakened at higher temperature.

3.2.7.3. Tempkin isotherm. It is based on the assumption that fall in heat of sorption is linear rather than logarithmic, as given in Freundlich equation [39]. It was suggested that due to sorbate/sorbent interactions the heat of sorption of all the molecules in the layer would decrease linearly with coverage [40]. The linear form of this isotherm can be given by

$$q_e = B \ln K_T + B \ln C_e \tag{11}$$

where C_e is concentration of the adsorbate at equilibrium (mg L^{-1}), q_e is the amount of adsorbate adsorbed at equilibrium (mg g^{-1}), $RT/b_T = B$ where T is the temperature (K), R is the ideal gas constant (8.314 J mol^{-1} K^{-1}), and K_T and b_T are constants. Linear plots of q_e vs. ln C_e (Figure not shown) enable the determination of constants K_T and B. The constant b_T is related to the heat of adsorption, and K_T is the equilibrium binding constant (L mg^{-1}) corresponding to the maximum binding energy. The values of K_T, b_T, and B are included in Table 2. Typical bonding energy range for ion-exchange mechanism is reported to be in the range of 8–16 kJ mol$^{-,1}$ while physisorption processes are reported to have adsorption energies less than –40 kJ mol^{-1} [41]. The lower value of b_T indicates that the interaction between dye CR and SBA-3 was weak. Hence, the adsorption process of CR onto SBA-3 can be expressed as physisorption, as indicated by the value of (b_T).

3.2.7.4. Dubinin–Radushkevich isotherm. The Dubinin–Radushkevich (D–R) isotherm equation is more general than the Langmuir isotherm because it does not assume a homogeneous surface or constant adsorption potential. It was applied to distinguish between the physical and chemical adsorption of dye [42]. The D–R model is postulated within adsorption space close to the adsorbent surface, which was applied to distinguish the nature of biosorption as physical or chemical [43]. The linear equations are given below:

$$\ln q_e = \ln q_s - B\,\varepsilon^2 \tag{12}$$

ε can be correlated as

$$\varepsilon = RT \ln (1 + 1/C_e) \tag{13}$$

where q_s (mg g^{-1}), D–R constant, is the maximum amount of adsorbate that can be adsorbed on adsorbent, the constant B gives the mean free energy E of sorption per molecule of sorbate when it is transferred to the surface of the solid from the bulk solution and can be computed using the following relationship

$$E = 1/(2B)^{1/2} \tag{14}$$

Mean adsorption energy calculated from D–R isotherm gives an idea about the chemisorptions or physisorption. For $E < 8$ kJ mol^{-1}, physisorption control the adsorption mechanism, while a value between 8 and 16 kJ mol^{-1} indicates involvement of chemisorptions process [44]. The values of E in the present system implied that physical adsorption may be one of the mechanisms for adsorption for dye CR. The values of constants are included in Table 2.

3.2.7.5. Non-ideal competitive adsorption (NICA) model. The model assumes that adsorption is a cooperative phenomenon, with the ligand binding ability at one site on the macromolecule, may influence different binding sites on the same macromolecule [45,46].

The linear form of the equation is:

$$\ln((q_{\max}/q_e) - 1) = \ln K_G - N \ \ln C_e \tag{15}$$

where K_G is the saturation constant (mg L^{-1}), N is the Hill cooperativity coefficient of the binding interaction, $N > 1$, positive cooperativity in binding, $N = 1$, noncooperative or hyperbolic binding, $N < 1$, negative cooperativity in binding. $q_{\max}$ is the maximum adsorption capacity of the adsorbent (mg g^{-1}). q_e (mg g^{-1}) and C_e (mg L^{-1}) are the equilibrium dye concentrations in the solid and liquid phase, respectively. The values of K_G and N are represented in Table 2. The value of N in this study is near to unity reflects non cooperative binding of adsorbent with adsorbate. The value of saturation constant (K_G) increases with temperature may ascribed to the speedy saturation at higher temperature.

3.2.8. Thermodynamic studies

Thermodynamic parameters are crucial for determining the spontaneity of an adsorption process. Thermodynamic parameters such as the changes in the free energy (ΔG), the enthalpy (ΔH), and the entropy (ΔS) associated with the adsorption process can be determined using the rate equation and the van't Hoff equation. The rate equation can be expressed as:

$$\Delta G = -RT \ln K_L \tag{16}$$

$$\Delta G = \Delta H - T \ \Delta S \tag{17}$$

From Eqs. (16) and (17), we get

$$\ln K_L = -\frac{\Delta H}{RT} + \frac{\Delta S}{R} \tag{18}$$

where K_L (L mol^{-1}) is the Langmuir constant, R is the universal gas constant (8.314 J mol^{-1} K^{-1}), and T is the absolute temperature (K). The values of ΔG and ΔH were obtained from the slope and intercept of the van't Hoff curve. The negative value of ΔG indicates that the sorption of CR on the adsorbent is spontaneous and feasible. The negative value of ΔH reflects the exothermic nature of the adsorption. The positive value of ΔS shows the increase in randomness at the interface during the adsorption process. Values of these parameters are mentioned in Table 3.

3.3. Error functions

Within recent decades, linear regression has been one of the most viable tools defining the best-fitting relationship [47], quantifying the distribution of adsorbates, mathematically analyzing the adsorption systems [48], and verifying the consistency and theoretical assumptions of an isotherm model [49]. In order to quantitatively compare the applicability of different isotherm models in fitting to data, four different error functions such as the sum of the absolute errors (SAE) [50], the average relative error (ARE) [51], the hybrid fractional error function (HYBRID) [52], and the Marquardt's percent standard deviation (MPSD) [53] were employed

$$\text{SAE} = \sum_{i=1}^{n} \left(\left|q_{e,\text{calc}} - q_{e,\text{exp}}\right|\right)_i \tag{19}$$

$$\text{ARE} = \frac{100}{n} \sum_{i=1}^{n} \left|\frac{q_{e,\text{calc}} - q_{e,\text{exp}}}{q_{e,\text{exp}}}\right|_i \tag{20}$$

$$\text{HYBRID} = \frac{100}{n-p} \sum_{i=1}^{n} \left[\frac{q_{e,\text{calc}} - q_{e,\text{exp}}}{q_{e,\text{exp}}}\right]_i \tag{21}$$

$$\text{MPSD} = 100 \sqrt{\frac{1}{n-p} \sum_{i=1}^{n} \left(\frac{(q_{e,\text{exp}} - q_{e,\text{calc}})}{q_{e,\text{exp}}}\right)_i^2} \tag{22}$$

Here, $q_{e,\text{cal}}$ and $q_{e,\text{exp}}$ are, respectively, the calculated and the experimental value of the equilibrium

Table 4
Isotherm error analysis for adsorption of CR onto SBA-3 at different temperatures

Error function	SAE	ARE	HYBRID	MPSD
303 K				
Langmuir	120.39	10.89	–4.22	15.68
Freundlich	56.27	3.18	0.118	4.88
Tempkin	48.87	3.09	1.45	5.15
D–R	60.89	4.00	3.31	7.14
NICA	22.90	1.48	0.097	2.58
313 K				
Langmuir	80.62	7.96	–2.20	13.00
Freundlich	31.89	1.95	0.033	3.09
Tempkin	30.44	2.12	1.05	3.68
D–R	48.62	3.39	4.75	7.02
NICA	10.26	0.71	0.02	1.22
323 K				
Langmuir	51.62	5.76	–2.98	9.52
Freundlich	16.69	1.23	0.033	2.18
Tempkin	17.34	1.39	0.59	2.81
D–R	42.66	3.47	1.75	6.10
NICA	15.52	1.19	0.067	2.18

adsorbate solid concentration in the solid phase (mg g^{-1}), n is the number of data points, and p is the number of parameters in the isotherm equation. The ARE function attempts to minimize the fractional error distribution across the entire concentration range. Values of all these error functions for isotherm models are listed in Table 4.

Values of error functioned shows that the equilibrium data are better represented by Freundlich isotherm.

4. Conclusion

This study investigates the removal efficiency of CR from aqueous solutions using mesoporous material SBA-3 as adsorbent. The rate of adsorption of the dye onto SBA-3 was very high, and equilibrium was attained within 15–30 min of contact for 60 mg L^{-1} whereas 100 min are sufficient for the removal of 200 mg L^{-1}. Adsorption kinetics analysis reveals that the adsorption is governed by pseudo-second-order model. Intraparticle diffusion analysis indicated that the process may be controlled by more than one mode of diffusion controlled mechanism. At low dye concentration, it is film diffusion whereas at higher concentration, particle diffusion is the prevalent one. Adsorption capacity (K_F) decreases with increase in temperature, which revealed the exothermic nature of adsorption process which is strengthened by decrease in values of monolayer capacity (C_m) and equilibrium binding constant (K_T). It is further confirmed by the negative value of enthalpy change (ΔH). Mean adsorption energy (E), n values of Freundlich, and b_T values of Temkin constant proved the physical nature of present adsorption system. The thermodynamic parameters insinuated that adsorption process is a feasible, spontaneous, exothermic, and entropically favorable. Langmuir model and R_L values supported the favorable adsorption. Maximum monolayer capacity was found to be 344.8 mg g^{-1} at 303 K.

References

[1] M. Rafatullah, O. Sulaimana, R. Hashima, A. Ahmad, Adsorption of methylene blue on low-cost adsorbents: A review, J. Hazard. Mater. 177 (2010) 70–80.
[2] A. Mittal, A. Malviya, D. Kaur, J. Mittal, L. Kurup, Studies on the adsorption kinetics and isotherms for the removal and recovery of Methyl Orange from wastewaters using waste materials, J. Hazard. Mater. 148 (2007) 229–240.
[3] A. Mittal, J. Mittal, A. Malviya, D. Kaur, V.K. Gupta, Adsorption of hazardous dye crystal violet from wastewater by waste materials, J. Colloid Interface Sci. 343 (2010) 463–473.
[4] A. Mittal, J. Mittal, L. Kurup, Adsorption isotherms, kinetics and column operations for the removal of hazardous dye, Tartrazine from aqueous solutions using waste materials—Bottom ash and de-oiled soya, as adsorbents, J. Hazard. Mater. B136 (2006) 567–578.
[5] A. Roy, B. Adhikari, S.B. Majumder, Equilibrium, kinetic, and thermodynamic studies of azo dye adsorption from aqueous solution by chemically modified lignocellulosic jute fiber, Ind. Eng. Chem. Res. 52 (2013) 6502–6512.
[6] C.L. Hsueh, Y.H. Huang, C.C. Wang, C.Y. Chen, Degradation of azo dyes using low iron concentration of Fenton and Fenton-like system, Chemosphere 58 (2005) 1409–1414.
[7] A. Mittal, V.K. Gupta, A. Malviya, J. Mittal, Process development for the batch and bulk removal and recovery of a hazardous, water-soluble azo dye (Metanil Yellow) by adsorption over waste materials (bottom ash and de-oiled soya), J. Hazard. Mater. 151 (2008) 821–832.
[8] A. Mittal, J. Mittal, A. Malviya, V.K. Gupta, Adsorptive removal of hazardous anionic dye congo red from wastewater using waste materials and recovery by desorption, J. Colloid Interface Sci. 340 (2009) 16–26.
[9] A. Afkhami, R. Moosavi, Adsorptive removal of congo red, a carcinogenic textile dye, from aqueous solutions by maghemite nanoparticles, J. Hazard. Mater. 174 (2010) 398–403.
[10] H. Daraei, A. Mittal, M. Noorisepehr, F. Daraei, Kinetic and equilibrium studies of adsorptive removal of phenol onto eggshell waste, Environ. Sci. Pollut. Res. 20 (2013) 4603–4611.
[11] M.M. Emamjomeh, M. Sivakumar, Review of pollutants removed by electrocoagulation and electrocoagulation/flotation processes, J. Environ. Manage. 90 (2009) 1663–1679.
[12] V.K. Gupta, I. Ali, T.A. Saleh, A. Nayak, S. Agarwal, Chemical treatment technologies for waste-water recycling—An overview, RSC Adv. 2 (2012) 6380–6388.
[13] V.K. Gupta, Suhas, Application of low-cost adsorbents for dye removal—A review, J. Environ. Manage. 90 (2009) 2313–2342.
[14] G. Crini, Non-conventional low-cost adsorbents for dye removal: A review, Bioresour. Technol. 97 (2006) 1061–1085.
[15] A. Mittal, V.K. Gupta, Adsorptive removal and recovery of hazardous azo dye eriochrome black T, Toxicol. Environ. Chem. 92 (2010) 1813–1823.
[16] A. Mittal, D. Kaur, J. Mittal, Batch and bulk removal of a triarymethane dye—Fast green FCF, from wastewater by adsorption over waste materials, J. Hazard. Mater. 163 (2009) 568–577.
[17] A. Mittal, D. Kaur, J. Mittal, Applicability of waste materials—Bottom ash and de-oiled soya, as adsorbents for the removal and recovery of a hazardous dye—Brilliant green, J. Colloid Interface Sci. 326 (2008) 8–17.
[18] A. Mittal, R. Jain, J. Mittal, M. Shrivastava, Adsorptive removal of hazardous dye quinoline yellow from waste water using coconut-husk as potential adsorbent, Fresenius Environ. Bull. 19 (2010) 1–9.
[19] D. Zhao, J. Feng, Q. Huo, N. Melosh, G. Fredrickson, B. Chmelka, Science 279 (1998) 548.

[20] M. Anbia, S. Salehi, Removal of acid dyes from aqueous media by adsorption onto amino-functionalized nanoporous silica SBA-3, Dyes Pigm. 94 (2012) 1–9.
[21] O.A. Anunziata, A.R. Beltramone, M.L. Martinez, L.L. Belon, Synthesis and characterization of SBA-3, SBA-15, and SBA-1 nanostructured catalytic materials, J. Colloid Interface Sci. 315 (2007) 184–190.
[22] R. Ahmad, R. Kumar, Adsorptive removal of congo red dye from aqueous solution using bael shell carbon, Appl. Surf. Sci. 257 (2010) 1628–1633.
[23] B. Qu, J. Zhou, X. Xiang, C. Zheng, H. Zhao, X. Zhou, Adsorption behavior of azo dye C. I. Acid Red 14 in aqueous solution on surface soils, J. Environ. Sci. 20 (2008) 704–709.
[24] V. Vadivelan, K.V. Kumar, Equilibrium, kinetics, mechanism and process design for the sorption of methylene blue onto rice husk, J. Colloid Interface Sci. 286 (2005) 90–100.
[25] P.S. Kumar, S. Ramalingam, C. Senthamarai, M. Niranjanaa, P. Vijayalakshmi, S. Sivanesan, Adsorption of dye from aqueous solution by cashew nut shell: Studies on equilibrium isotherm, kinetics and thermodynamics of interactions, Desalination 261 (2010) 52–60.
[26] Z. Al-Qodah, Adsorption of dyes using shale oil ash, Water Res. 34 (2000) 4295–4303.
[27] G. Blazquez, F. Hernainz, M. Calero, L.F. Ruiz-Nunez, Removal of cadmium ions with olive stones: The effect of some parameters, Process Biochem. 40 (2005) 2649–2654.
[28] C.Y. Chang, W.T. Tsai, C.H. Ing, C.F. Chang, Adsorption of polyethylene glycol (PEG) from aqueous solution onto hydrophobic zeolite, J. Colloid Interface Sci. 260 (2003) 273–279.
[29] M.J. Weber, J. Morris, Kinetic of adsorption on carbon from solution, J. Sanit. Eng. Div. ASCE 89 (1963) 31–59.
[30] A. Ahmada, M. Rafatullahb, O. Sulaimanb, M.H. Ibrahim, R. Hashim, Scavenging behaviour of meranti sawdust in the removal of methylene blue from aqueous solution, J. Hazard. Mater. 170 (2009) 357–365.
[31] B.H. Hameed, M.I. El-Khaiary, Malachite green adsorption by rattan sawdust: Isotherm, kinetic and mechanism modeling, J. Hazard. Mater. 159 (2008) 574–579.
[32] G.E. Boyd, A.W. Adamson, L.S. Meyers, The exchange adsorption of ions from aqueous solution by organic zeolites II Kinetics, J. Am. Chem. Soc. 69 (1947) 2836–2848.
[33] D. Reichenberg, Properties of ion exchange resins in relation to their structure. III. Kinetics of exchange, J. Am. Chem. Soc. 75 (1953) 589–597.
[34] S. Wang, H. Li, L. Xu, Application of zeolite MCM-22 for basic dye removal from wastewater, J. Colloid Interface Sci. 295 (2006) 71–78.
[35] M. Ozacar, I.A. Sengil, A kinetic study of metal complex dye sorption onto pine sawdust, Process Biochem. 40 (2005) 565–572.
[36] C. Aharoni, S. Sideman, E. Hoffer, Adsorption of phosphate ions by colloid ion-coated alumina, J. Chem. Technol. Biotechnol. 29 (1979) 404–412.
[37] E. Tutem, R. Apak, C.F. Unal, Adsorptive removal of chlorophenols from water by bituminous shale, Water Res. 32 (1998) 2315–2324.
[38] A.S. Ozcan, B. Erdem, A. Ozcan, Adsorption of Acid Blue 193 from aqueous solutions onto BTMA-bentonite, Colloids Surf., A 266 (2005) 73–81.
[39] C. Aharoni, M. Ungarish, Kinetics of activated chemisorption. Part 2. Theoretical models, J. Chem. Soc. Faraday Trans. 73 (1977) 456–464.
[40] M. Hosseini, S.F.L. Mertens, M. Ghorbani, M.R. Arshadi, Asymmetrical schiff bases as inhibitors of mild steel corrosion in sulphuric acid media, Mater. Chem. Phys. 78 (2003) 800–807.
[41] B. Kiran, A. Kaushik, Chromium binding capacity of Lyngbya putealis exopolysaccharides, Biochem. Eng. J. 38 (2008) 47–54.
[42] F. Kargi, S. Ozmihci, Biosorption performance of powdered activated sludge for removal of different dyestuff, Enzyme Microb. Technol. 35 (2004) 267–271.
[43] T. Akar, I. Tosun, Z. Kaynak, E. Kavas, G. Incirkus, S.T. Akar, Assessment of the biosorption characteristics of a macro-fungus for the decolorization of acid red 44 dye, J. Hazard. Mater. 171 (2009) 865–871.
[44] A. Mittal, J. Mittal, A. Malviya, V.K. Gupta, Removal and recovery of Chrysoidine Y from aqueous solutions by waste materials, J. Colloid Interface Sci. 344 (2010) 497–507.
[45] O. Gercel, H.F. Gercel, A.S. Koparal, U.B. Ogutveren, Removal of disperse dye from aqueous solution by novel adsorbent prepared from biomass plant material, J. Hazard. Mater. 160 (2008) 668–674.
[46] L.K. Koopal, W.H. Van Riemsdijk, D.G. Kinniburgh, Humic matter and contaminants. General aspects and modelling ion binding, Pure Appl. Chem. 73 (2001) 2005–2016.
[47] K.V. Kumar, Comparative analysis of linear and non-linear method of estimating the sorption isotherm parameters for malachite green onto activated carbon, J. Hazard. Mater. 136 (2006) 197–202.
[48] D.H. Lataye, I.M. Mishra, I.D. Mall, Adsorption of 2-picoline onto bagasse fly ash from aqueous solution, Chem. Eng. J. 138 (2008) 35–46.
[49] B. Boulinguiez, P. Le Cloirec, D. Wolbert, Revisiting the determination of Langmuir parameters application to tetrahydrothiophene adsorption onto activated carbon, Langmuir 24 (2008) 6420–6424.
[50] R.K. Rajoriya, B. Prasad, I.M. Mishra, K.L. Wasewar, Adsorption of benzaldehyde on granular activated carbon: Kinetics, equilibrium, and thermodynamic, Chem. Biochem. Eng. Q. 21 (2007) 219–226.
[51] A. Kapoor, R.T. Yang, Correlation of equilibrium adsorption data of condensible vapours on porous adsorbents, Gas Sep. Purif. 3 (1989) 187–192.
[52] J.F. Porter, G. Mckay, K.H. Choy, The prediction of sorption from a binary mixture of acidic dyes using single- and mixed-isotherm variants of the ideal adsorbed solute theory, Chem. Eng. Sci. 54 (1999) 5863–5885.
[53] S. Chowdhury, P. Saha, Adsorption kinetic modeling of safranin onto rice husk biomatrix using pseudo-first- and pseudo second- order kinetic models: Comparison of linear and non-linear method, Clean Soil Air Water 39 (2011) 274–282.